Investigation of the Robustness of Nanoelectronic Structures Based on Resonant Tunneling Elements

Bondarev A.V.
Department of of industrial power supply
Kumertau branch of Orenburg State University
Kumertau, Russia
bondarevav@kfosu.edu.ru

Efanov V.N.
Department of electronics and biomedical technologies
Ufa State Aviation Technical University
Ufa, Russia
efanov@mail.ru

***Abstract*— We consider the problem of assessing the stability of nanoelectronic structures, which include resonant tunneling elements. Research shows that multi-input logic gates based on two-level logic cells MOBILE have a short (picosecond) switching time and higher functionality due to the ability to implement logic functions with fewer gates. This creates good prospects for the development of ultra-high-performance programmable logic device (PLD) with a high degree of integration, which are required for organizing high-performance computing. However, the extremely high sensitivity of resonant tunneling elements to changes in the energies of quantum states requires an assessment of the stability of such structures to external influences in real operation. For this purpose, a technique is proposed for investigating the robustness of logic cells MOBILE based on a resonant tunneling diode and an HBT transistor**

Keywords*— *nanoelectronic structures, resonant tunneling diode, two-level logic cell, interpolation formula, structural-parametric model, interval analysis, computational algorithm

I. INTRODUCTION

The development of devices based on nanoelectronic structures is a relevant and dynamically developing field of science. Interest in this area is associated both with fundamentally new fundamental scientific problems and physical phenomena, and with the prospects for the creation of new quantum devices and systems with wide functional capabilities on the basis of already discovered phenomena. The use of devices, in the functioning of which quantum effects play a key role, can significantly increase the performance of computing systems, increase the throughput of communication channels, dramatically increase the information capacity and quality of information display systems with a simultaneous decrease in energy consumption; significantly increase the sensitivity of sensor devices and expand the range of measured values; create highly efficient solid-state lighting devices; and also to increase the proportion of the use of electronic and optoelectronic components in medical, biological, chemical, mechanical engineering and other technologies [1]-[5].

The element base, based on the use of various low-dimensional structures, is the most promising for electronic technology of new generations. However, in the transition to systems of the nanometer range, the quantum-mechanical nature of quasiparticles in a solid begins to manifest itself clearly. As a result, a number of problems arise when using nanoelectronic structures in radioelectronic systems. These problems are mainly associated with both the design of such structures and with ensuring the operability of such devices in real-life conditions [6]. Electronic systems must operate at low or high temperatures, vibration, electromagnetic fields, etc. In this regard, the task is to assess the performance of nanoelectronic devices when external influences change in a wide range. Such an assessment should be carried out at all stages of the development of the device, including during its circuit design.

II. ANALYSIS OF PHYSICAL PROCESSES IN NANOELECTRONIC STRUCTURES BASED ON RESONANT TUNNELING ELEMENTS

Physical processes in resonant tunneling diodes (RTD) and resonant tunneling transistors are based on the effect of tunneling of charge carriers through a potential barrier. In this case, tunneling in nanoelectronic structures has features associated with the wave properties of carriers and with the quantization of their energy states. In this connection, the tunneling of carriers in nanostructures depends not only on the parameters of potential barriers, but also on the allowed energy states for carriers in these structures. If the Fermi level of the injecting electrode coincides with the discrete level of the structure limited by barriers, a sharp increase in the tunneling current is observed — the phenomenon of resonant tunneling. In this case, a region with a negative differential resistance appears on the current-voltage characteristic. In fig. 1 shows the current-voltage characteristic of a resonant tunneling diode (RTD). It is a tunnel structure composed of successive quantum wells that are separated by potential barriers. Usually, a structure with one well and two barriers is used, since with a large number of wells, it is difficult to match the resonant electron transfer [7]. The double-barrier structure is usually made of GaAS / AlGaAs superlattices. The electrodes and quantum well are formed from GaAs, and the barriers are formed from the GaAlAs compound.

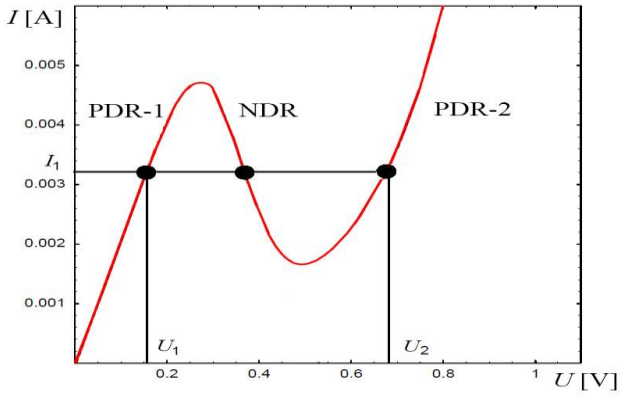

Fig. 1. Current-voltage characteristic of the double-barrier structure

The current-voltage characteristic contains three different working areas: positive differential resistance PDR-1, PDR-2

978-1-6654-3941-1 @2021 IEEE

and negative differential resistance NDR. Two PDR regions are stable working regions, and NDR region is metastable. Such devices, which have a section of negative differential resistance, are called negatrons [8]. In negatrons, there are two defined stable voltage values for each current value. In fig. 1 for current I_1 is voltage U_1 and U_2. The RTD state at voltage U_1 is considered a low-resistance or "open" state, and the U_2 state is a high-resistance or "closed" state. Switching of such circuits is provided due to the difference in the peak currents of the RTD, which, when the bias voltage is applied, leads to the "shutdown" of the RTD with a low current, and the RTD with a high current remains in the "open" state.

The significant nonlinearity of the current-voltage characteristics of negatrons determines the following advantages of devices of this class:

- short (picosecond) switching time;
- higher functionality of RTD in comparison with traditional elements due to the ability to implement similar functions with fewer elements.

However, the presence of internal instability and the possibility of spontaneous generation of electrical oscillations leads to the fact that electrical circuits, which are built only on negatrons, are unstable. The stability problem is solved through the use of a two-level logical cell MOBILE (MOnostable-to-BIstable transition Logic Element) [9]. In the simplest case, such a cell contains two series-connected RTDs (Goto pair) or a combination of a two-pole RTD and three-pole HEMT and HBT transistors.

In a pair of Goto (Fig. 2, *a*), one RTD acts as a load, and the other as an active element. Switching in such circuits is provided by the difference in the peak currents of the RTD. When the bias voltage is applied, this causes the low current RTD to "turn off", while the high current RTD remains in the "open" state. By controlling the peak current of an active RTD, either a stable low level or a stable high level can be obtained at the output of the Goto pair.

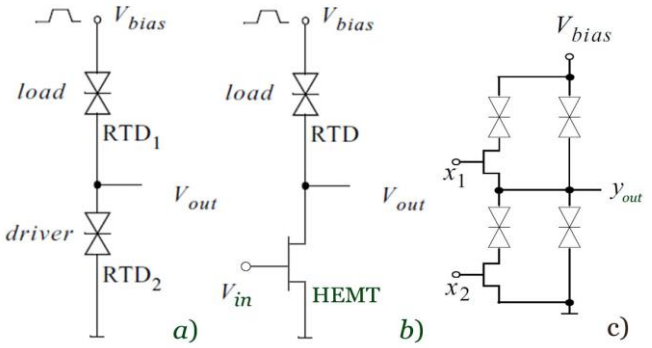

Fig. 2. Two-level logical cells MOBILE: *a*) Goto pair; *b*) a combination of RTD and HEMT transistor; *c*) multi-input logic element

In an inverter based on an HEMT transistor with an RTD load (Fig. 2, *b*), a bistable configuration occurs if V_{bias} is twice the peak voltage. This results in two self-stabilizing digital output states. If V_{in} corresponds to "1" and the transistor turns on, then the RTD goes into a high-resistance state, i.e. to the second ascending region current-voltage characteristic, and the output voltage goes low. When feeding "0", i.e. when the transistor is closed, the RTD switches to a low impedance state and the output voltage goes high.

On the basis of standard cells MOBILE, ultra-fast multi-input logical elements are created. Their functionality allows you to implement any logical function by expanding the basic configuration with both serial and parallel blocks. In fig. 2, c) shows a diagram of a two-input threshold gate for performing threshold logic functions.

The developed logical elements MOBILE serve as the basis for creating programmable logic integrated device (PLD), which have low power consumption and small topological dimensions at high current densities. Currently, there is an increased interest in the use of PLDs with a high degree of integration in various branches of technology, especially where high-performance computing is required.

The fact is that the real performance of multiprocessor systems that combine microprocessors with traditional architecture often does not exceed 10-15% of the declared peak performance. This is due to the need to implement a variety of interprocessor exchange procedures, as well as synchronize sequential processes running in the system processors. The main reason for this is the discrepancy between the rigid architecture of computing systems and the information structure of tasks. To eliminate this drawback, it is proposed to use a method for constructing a computing system with a flexible dynamically programmable architecture, which is adjusted to the information structure of a specific task. Previously, the practical implementation of this concept was restrained by the lack of an element base necessary for the implementation of a reconfigurable architecture. This opportunity appears when using PLDs, the configuration of which can be changed, thereby adapting the computing system to solve a specific type of problem.

In this regard, the hardware implementation of the SWARM program parallel execution system, which is being developed within the DARPA UHPC program and designed to support the execution time in large heterogeneous computing systems, involves the use of PLDs. PLDs are at the heart of Novo-G, one of the highest performing supercomputers with reconfiguration, (University of Florida, USA). Novo-G has a total of 192 Altera Stratix-III E260 gate arrays, each of which contains 768 multipliers (18x18), 254 thousand gates, 204 thousand registers and has 4.25 GB of memory. Another notable example of a multifunctional reconfigurable system that uses PLDs is the Convey HC-1ex system from Convey Computer. For reprogramming, the user has four cards available for executing custom programs, into which you can load either your own firmware, or use one of the specialized applications (financial analysis, bioinformatics, speech recognition, graph tasks, etc.).

However, for widespread introduction of PLDs based on resonant tunneling devices, it is necessary to ensure their stable operation in a wide range of external influences. The point is that resonant tunneling is extremely sensitive to changes in the energies of quantum states in nanostructures. In this case, the energies of quantum states are determined by the distribution of the concentration of current carriers. Low-dimensional systems used in resonant tunneling devices are open systems with a variable number of particles. In such systems, thermodynamic equilibrium is established by the exchange of particles between tunnel-coupled electronic systems. This interaction must be taken into account when describing quantum transport in nanostructures. The interaction between systems of current carriers can manifest

itself in joint plasma excitations or correlation multiparticle phenomena, which can affect the distribution of the tunneling current in the structure and its magnitude. The existing methods for assessing the sensitivity make it possible to evaluate the behavior of devices in a small vicinity of the nominal operating mode. This raises the problem of analyzing the robustness of radio electronic systems. The solution to this problem will make it possible to study the influence of the interaction of electronic systems on quantum transport in nanostructures and to evaluate the behavior of micro- and nanoelectronic devices when external influences change over a wide range. For this purpose, we will form a generalized structural-parametric model of hybrid radio-electronic systems based on micro- and nanoelectronic components, taking into account the influence of uncertain factors of the external and internal environment.

III. ANALYTICAL MODEL OF A RESONANT TUNNELING DIODE

We will begin the development of a generalized structural-parametric model of logical cells MOBILE with the construction of a model of a resonant tunneling diode. In [10], an exact model of RTD is given, which consists of a combination of a quantum capacitance $C(U)$ and a nonlinear resistance $R(U)$ (Fig. 3).

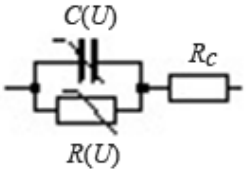

Fig. 3. Large-Signal-Based Nonlinear Model for a Resonant Tunneling Diode

Quantum capacitance describes the change in charge in a quantum well. Series resistance R_C is due to the contact and distributed resistance of the semiconductor. Model parameters for three different areas at typical offset are shown in Table I.

TABLE I. RTD PARAMETERS

Current-voltage characteristic area, offset, V	PDR1, 0.2	NDR, 1.0	PDR2, 1.3
R, Ohm	255.9	-504.4	132.1
C, fF (10^{-5} F)	40.8	69.1	43.8

As shown earlier, the current-voltage characteristic of a resonant tunneling diode contains a number of characteristic sections corresponding to the positive and negative values of the differential resistance of the device. In this regard, when constructing a mathematical model of a resonant tunneling diode, we use piecewise polynomial interpolation of its current-voltage characteristic.

To ensure high accuracy of the RTD current-voltage characteristic description, it is necessary to specify a large number of interpolation nodes. When using the classical interpolation formulas of Newton, Bessel, Stirling, etc. this leads to the need to operate with high-order interpolation polynomials. As studies show, in this case the interval of uniform convergence of interpolation polynomials to the interpolated function is significantly reduced. The lack of uniform convergence means that the interpolation problem becomes ill-posed in the sense of Hadamard. As a consequence, minor modifications to the original data can lead to a significant change in the interpolation result. This contradiction can be eliminated using piecewise polynomial interpolation, when the original interval $[a,b]$ is divided into smaller segments, on each of which its own polynomial of small degree is used. In this work, we will use cubic splines. The initial current-voltage characteristic $I(U)$ is shown in Fig. 4, a). This characteristic was obtained at room temperature for an RTD with the following structure: InAs/$In_{0.53}Ga_{0.47}As$/AlAs on an InP substrate (3x3 μm^2) [11].

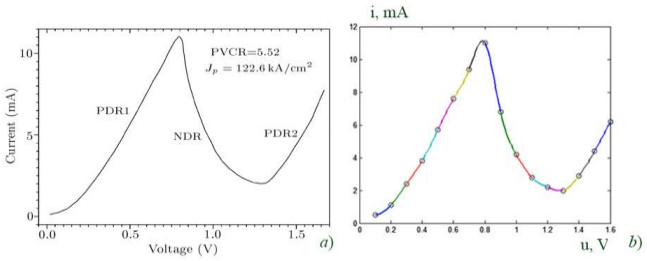

Fig. 4. Interpolation of the current-voltage characteristics of the RTD: *a*) experimental characteristics; *b*) the result of interpolation

For interpolation, we chose a voltage interval from 0.1 V to 1.6 V. We divide this interval into 16 segments with a step of 0.1:

$$0.1 = a = u_0 < u_1 < \ldots < u_{14} < u_{15} = b = 1.6. \qquad (1)$$

The values of the current $i_k = I(u_k),\ k = 0,1,\ldots,15$ found at the interpolation nodes are given in Table II.

TABLE II. INITIAL DATA

k	0	1	2	3	4	5	6	7	8	9	10	11	12	13	14	15
u_k, V	0.1	0.2	0.3	0.4	0.5	0.6	0.7	0.8	0.9	1	1.1	1.2	1.3	1.4	1.5	1.6
i_k, mA	0.5	1.1	2.4	3.8	5.7	7.6	9.4	11	6.8	4.2	2.8	2.2	2	2.9	4.4	6.2

On each segment $[u_{k-1},u_k],\ k = 1,2,\ldots,15$, it is necessary to find a spline function $s(u) = s_i(u)$ that satisfies the following conditions:

1) the function $s(u)$ is a cubic polynomial on each segment $[u_{k-1},u_k],\ k = 1,2,\ldots,15$;

2) the function $s(u)$ is continuous on the segment [0.1; 1.6], like its first and second derivatives;

3) coincidence in interpolation nodes: $s(u_k) = I(u_k),\quad k = 0,1,2,\ldots,15$.

A function $s(x)$ that satisfies conditions 1) - 3) is a third degree polynomial:

$$s_k(u) = a_k + b_k(u - u_k) + \frac{c_k}{2}(u - u_k)^2 + \frac{d_k}{6}(u - u_k)^3, \qquad (2)$$
$$u_{k-1} \le u \le u_k,\quad k = 1,2,\ldots,15,$$

where a_k, b_k, c_k, d_k - is the coefficients of the polynomial to be found.

Coefficients c_k with satisfy the following system of equations

$$c_0 = c_{15} = 0;$$
$$h_k c_{k-1} + 2(h_k + h_{k+1})c_k + h_{k+1}c_{k+1} = 6\left(\frac{i_{k+1} - i_k}{h_{k+1}} - \frac{i_k - i_{k-1}}{h_k}\right), \quad (3)$$
$$k = 1,2,...,14,$$

here $h_k = u_k - u_{k-1}$.

The system of equations (3) has a unique solution, since the coefficient matrix is tridiagonal. Using the found coefficients c_k, the remaining coefficients are determined by the following formulas:

$$a_k = I(u_k); \; d_k = \frac{c_k - c_{k-1}}{h_k};$$
$$b_k = \frac{h_k}{2}c_k - \frac{h_k^2}{6}d_k + \frac{i_k - i_{k-1}}{h_k}; \; k = 1,2,...,15. \quad (4)$$

The calculation results are shown in Table III.

TABLE III. COEFFICIENTS OF INTERPOLATION POLYNOMIALS

k	1	2	3	4	5	6	7	8	9	10	11	12	13	14
a_k	1.1	2.4	3.8	5.7	7.6	9.4	11	6.8	4.2	2.8	2.2	2	2.9	4.4
b_k	-1.5	1.1	0.9	-3.2	-3	3.6	2.3	-0.2	2.7	1.8	1.5	0.9	-1.5	0.2
c_k	3.8	0.5	-0.7	-20	21	-4.6	-8.5	5.7	1.5	-5.7	5.4	-6.4	2.3	-0.1
d_k	-1.8	-0.5	-32	69	-21	-13	5.3	-3.5	-12	2.9	-7.9	4.8	-1	0.04

The result of piecewise polynomial interpolation of the current-voltage characteristic by cubic splines is shown in Fig. 4, *b*). Using the obtained result, we construct a generalized structural-parametric model for evaluating the robustness of MOBILE logical cells.

IV. STRUCTURAL-PARAMETRIC MODEL OF AN HBT-BASED INVERTER WITH AN RTD LOAD

Let us consider the technique of investigating the robustness of MOBILE logic cells using the example of an inverter (Fig. 2, b). This two-level logic cell contains a series-connected RTD and NVT transistor. The equivalent circuit of this cell is shown in Fig. 5, a).

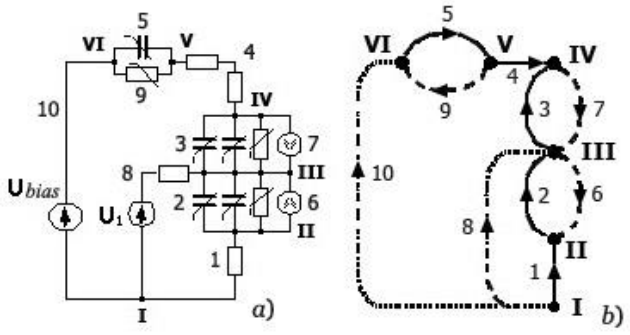

Fig. 5. Topological analysis of the inverter: a) the equivalent circuit of the inverter; b) topological graph of a multipole

The circuit contains the RTD model and the Ebers-Moll model for the NVT transistor. This nonlinear reactive multipole can be described using a system of nonlinear differential equations. To ensure the fulfillment of the conditions for the algorithmic solvability of such a system of equations, we carry out a topological and parametric analysis of the equivalent circuit. We construct a topological graph of a multipole (Fig. 5, *b*) and find the main topological matrices: A - the matrix of principal sections, B - matrix of principal contours:

$$A = \begin{bmatrix} 1 & 0 & 0 & 0 & 0 & 0 & 0 & 1 & 0 & 1 \\ 0 & 1 & 0 & 0 & 0 & -1 & 0 & 1 & 0 & 1 \\ 0 & 0 & 1 & 0 & 0 & 0 & -1 & 0 & 0 & 1 \\ 0 & 0 & 0 & 1 & 0 & 0 & 0 & 0 & 0 & -1 \\ 0 & 0 & 0 & 0 & 1 & 0 & 0 & 0 & -1 & -1 \end{bmatrix};$$

$$B = \begin{bmatrix} 1 & 0 & 0 & 0 & 0 & 0 & 0 & 1 & 0 & 1 \\ 0 & 1 & 0 & 0 & 0 & -1 & 0 & 1 & 0 & 1 \\ 0 & 0 & 1 & 0 & 0 & 0 & -1 & 0 & 0 & 1 \\ 0 & 0 & 0 & 1 & 0 & 0 & 0 & 0 & 0 & -1 \\ 0 & 0 & 0 & 0 & 1 & 0 & 0 & 0 & -1 & -1 \end{bmatrix}.$$

Let us write the system of topological equations with respect to the vectors of deviations ΔI and ΔU of currents and voltages in the disturbed mode I_o, U_o from their values I_n, U_n in the nominal operating mode

$$A\Delta I = 0; \; B\Delta U = 0. \quad (5)$$

Let us select in the composition of the vectors ΔI and ΔU the components that correspond to the following types of branches: reactive (capacitive) ribs, linear resistive ribs, nonlinear resistive chords, linear resistive chords. The vectors ΔI and ΔU ordered in a similar way take the form

$$\Delta I = \left\lfloor \Delta I_C^P; \Delta I_R^P; \Delta I_H^X; \Delta I_R^X \right\rfloor;$$
$$\Delta U = \left\lfloor \Delta U_H^X; \; \Delta U_R^X; \; \Delta U_C^P; \; \Delta U_R^P \right\rfloor.$$

In this case, the following block form of notation corresponds to topological matrices

$$A = \left[\begin{array}{c|c|c|c} \vec{I} & 0 & A_H^C & A_R^C \\ \hline 0 & \vec{I} & A_H^R & A_R^R \end{array}\right]; \; B = \left[\begin{array}{c|c|c|c} \vec{I} & 0 & B_C^H & B_R^H \\ \hline 0 & \vec{I} & B_C^R & B_R^R \end{array}\right].$$

As a result of the decomposition performed, the system of topological equations (5) is divided into five groups of equations

$$\Delta I_C^P = -A_H^C \Delta I_H^X - A_R^C \Delta I_R^X; \; \Delta U_H^X = -B_C^H \Delta U_C^P - B_R^H \Delta U_R^P;$$
$$\Delta I_R^P = -A_H^R \Delta I_H^X - A_R^R \Delta I_R^X; \; \Delta U_R^X = -B_C^R \Delta U_C^P - B_R^R \Delta U_R^P.$$

Combining the vectors of voltage and current deviations for linear resistive branches allows you to form the following hybrid system of equations

$$\Delta I_C^P = -A_H^C \Delta I_H^X + \left[0 \; \vdots \; -A_R^C\right] \begin{bmatrix} \Delta U_R^P \\ \Delta I_R^X \end{bmatrix}; \quad (6)$$

$$\Delta U_H^X = -B_C^H \Delta U_C^P + \left[-B_R^H \; \vdots \; 0\right] \begin{bmatrix} \Delta U_R^P \\ \Delta I_R^X \end{bmatrix}; \quad (7)$$

$$\begin{bmatrix} \Delta U_R^X \\ \Delta I_R^P \end{bmatrix} = \begin{bmatrix} -B_C^R \\ 0 \end{bmatrix} \Delta U_C^P + \begin{bmatrix} 0 \\ -A_H^R \end{bmatrix} \Delta I_H^X + \left[\begin{array}{c|c} -B_R^R & 0 \\ 0 & -A_R^R \end{array}\right] \begin{bmatrix} \Delta U_R^P \\ \Delta I_R^X \end{bmatrix}. \quad (8)$$

The next step in the model building procedure is to obtain parametric equations. The parametric equations for the electric branches of the equivalent circuit of the inverter, taking into account the finite increments of their parameters,

are found on the basis of the analysis of disturbed states that are caused by the influence of external and internal factors.

For a linear resistor $u_R(t) = Ri_R(t)$, the perturbed state equation has the following form

$$u_R(t) + \Delta u_R(t) = (R+\Delta R)[i_R(t) + \Delta i_R(t)] =$$
$$= Ri_R(t) + \Delta Ri_R(t) + R\Delta i_R(t) + \Delta R\Delta i_R(t).$$

As a result, the equation in deviations will be as follows:

$$\Delta u_R(t) = E_R^{\text{ind}} + R_{\text{equ}}\Delta i_R(t) \quad (9)$$

where $E_R^{\text{ind}} = \Delta Ri_R(t)$ is an independent voltage source, the value of which belongs to a given range of values, $R_{\text{equ}} \in [R+\Delta R;\ \ R-\Delta R]$ - is the equivalent resistance of the resistor for the disturbed mode, the value of which is also interval.

Similarly, for a resistor, which is given by its conductivity, the equation in deviations has the form

$$\Delta i_R(t) = J_R^{\text{ind}} + Y_{\text{equ}}\Delta u_R(t). \quad (10)$$

For nonlinear resistors and nonlinear capacitances, we will use the parametric equations in deviations, which were obtained in [11]

$$\Delta u_H(t) = E_H^{\text{ind}} + Z_{\text{equ}}(\Delta i_H, J_{\text{dep}}) \quad (11)$$

where E_H^{ind} - is an interval independent voltage source, $Z_{\text{equ}}(\Delta i_H, J_{\text{dep}})$ - is a nonlinear resistance, J_{dep} - is a dependent, current-controlled, current source.

$$\Delta i_C(t) = J_C^{\text{ind}} + J_C^{\text{dep}}(\Delta u_C) + Y_C^{\text{equ}}(\Delta u_C) + C_{\text{equ}}(\Delta u_C)\frac{d\Delta u_C}{dt}. \quad (12)$$

Here J_C^{ind} - is an independent current source, $J_C^{\text{dep}}(\Delta u_C)$ - is a dependent interval current source, $Y_C^{\text{equ}}(\Delta u_C)$ - is an equivalent, nonlinear and interval, conductivity, $C_{\text{equ}}(\Delta u_C)$ is an equivalent, nonlinear and interval, capacitance.

Using expressions (9)-(12), we form the vectors of current increments for capacitive ribs, voltage increments for nonlinear resistive chords, current and voltage increments for linear resistive ribs and chords

$$\Delta I_C^P = J_C^P + J_C^P(\Delta U_C^P) + Y_C^P(\Delta U_C^P) + C_P(\Delta U_C^P)\frac{d\Delta U_C^P}{dt}, \quad (13)$$

where $J_C^P,\ J_C^P(\Delta U_C^P),\ Y_C^P(\Delta U_C^P)$ - is column vectors of independent and dependent current sources, as well as nonlinear conductivities, $C_P(\Delta U_C^P)$ - is a diagonal matrix of equivalent capacitances.

$$\Delta U_H^X = E_H^X + Z_X(\Delta I_H^X), \quad (14)$$

where $E_H^X,\ Z_X(\Delta I_H^X)$ - is vector-columns of independent voltage sources and nonlinear resistances.

$$\begin{bmatrix}\Delta U_R^X \\ \Delta I_R^P\end{bmatrix} = \begin{bmatrix}E_R^X \\ J_R^P\end{bmatrix} + \left[\begin{array}{c|c} 0 & R_X \\ \hline Y_P & 0\end{array}\right]\begin{bmatrix}\Delta U_R^P \\ \Delta I_R^X\end{bmatrix}, \quad (15)$$

where $E_R^X,\ J_R^P$ - is vector-columns of independent voltage and current sources, R_X, Y_P - diagonal matrixes of resistance and conductivity.

Substitute, further, (13), (14), (15), respectively, in (6), (7), (8)

$$J_C^P + J_C^P(\Delta U_C^P) + Y_C^P(\Delta U_C^P) + C_P(\Delta U_C^P)\frac{d\Delta U_C^P}{dt} =$$
$$= -A_H^C\Delta I_H^X + \left[0 \mid -A_R^C\right]\begin{bmatrix}\Delta U_R^P \\ \Delta I_R^X\end{bmatrix};$$

$$E_H^X + Z_X(\Delta I_H^X) = -B_C^H\Delta U_C^P + \left[-B_R^H \mid 0\right]\begin{bmatrix}\Delta U_R^P \\ \Delta I_R^X\end{bmatrix};$$

$$\begin{bmatrix}E_R^X \\ J_R^P\end{bmatrix} + \left[\begin{array}{c|c} 0 & R_X \\ \hline Y_P & 0\end{array}\right]\begin{bmatrix}\Delta U_R^P \\ \Delta I_R^X\end{bmatrix} =$$
$$= \begin{bmatrix}-B_C^R \\ 0\end{bmatrix}\Delta U_C^P + \begin{bmatrix}0 \\ -A_H^R\end{bmatrix}\Delta I_H^X + \left[\begin{array}{c|c} -B_R^R & 0 \\ \hline 0 & -A_R^R\end{array}\right]\begin{bmatrix}\Delta U_R^P \\ \Delta I_R^X\end{bmatrix}.$$

After transformation we get

$$\frac{d\Delta U_C^P}{dt} = F_C^P(\Delta U_C^P) + V_1^C\Delta I_H^X + V_2^C\begin{bmatrix}\Delta U_R^P \\ \Delta I_R^X\end{bmatrix} + V_3^C J_C^P, \quad (16)$$

here $F_C^P(\Delta U_C^P) = \left[C_P(\Delta U_C^P)\right]^{-1}\left[J_C^P(\Delta U_C^P) + Y_C^P(\Delta U_C^P)\right]$;

$V_1^C = -\left[C_P(\Delta U_C^P)\right]^{-1}A_H^C$; $V_2^C = \left[C_P(\Delta U_C^P)\right]^{-1}\left[0 \mid -A_R^C\right]$;

$V_3^C = \left[C_P(\Delta U_C^P)\right]^{-1}J_C^P$.

$$Z_X(\Delta I_H^X) = -B_C^H\Delta U_C^P + \left[-B_R^H \quad 0\right]\begin{bmatrix}\Delta U_R^P \\ \Delta I_R^X\end{bmatrix}E_H^X; \quad (17)$$

$$\left[\begin{array}{c|c} B_R^R & R_X \\ \hline Y_P & A_R^R\end{array}\right]\begin{bmatrix}\Delta U_R^P \\ \Delta I_R^X\end{bmatrix} = \begin{bmatrix}-B_C^R \\ 0\end{bmatrix}\Delta U_C^P + \begin{bmatrix}0 \\ -A_H^R\end{bmatrix}\Delta I_H^X + \begin{bmatrix}E_R^X \\ J_R^P\end{bmatrix}. \quad (18)$$

Thus, the structural-parametric model (16) - (18) of the device under consideration is a set of interval ordinary differential equations, interval nonlinear and linear algebraic equations.

The algorithmic solvability of the resulting model is due to its structure, which allows the stepwise integration of differential equations and the solution of algebraic equations at each step of integration.

In this case, the sought parameters $\Delta = [\Delta U_C^P; \Delta U_R^P; \Delta I_H^X; \Delta I_R^X]$ are interval functions of $\Delta_i \in [\underline{\Delta_i}; \overline{\Delta_i}]$. In this regard, the task is to estimate the range of values of these parameters Δ_i. This area is defined by the following set $range(\Delta_i; \Xi) = \{\Delta_i(\xi) | \xi \in \Xi\}$. As follows from [12], the calculation of interval expansions of the coefficients Δ_i based only on the boundaries of the intervals of the vector Ξ, allows you to learn only the interval shell, which is an external interval estimate of these coefficients. The quality of such an assessment is determined by the following inequalities

$$dist(range(\Delta_i; \Xi), \Delta_i(\xi)) \le \gamma \|wid\,\xi\|_\infty, \quad \gamma \ge 0 \quad (19)$$
$$wid\,\Delta_i(\xi) \le \delta\|wid\,\xi\|_\infty, \quad \delta \ge 0.$$

where $dist(\xi_1, \xi_2)$ is the Hausdorff distance between intervals $\xi_1 = [\underline{\xi_1}, \overline{\xi_1}]$ and $\xi_2 = [\underline{\xi_2}, \overline{\xi_2}]$, which is defined as $dist(\xi_1, \xi_2) = \max\{|\underline{\xi_1} - \underline{\xi_2}|, |\overline{\xi_1} - \overline{\xi_2}|\}$; $wid\,\xi = \overline{\xi} - \underline{\xi}$ is the width of the corresponding interval.

The main reason for extending interval estimates is the fact that standard interval arithmetic is a commutative semigroup in which the subdistributive law is satisfied instead of the distributive law. To eliminate such a disadvantage, it is proposed to use a broader and more complete algebraic system, which is called Kaucher's interval arithmetic [13]. Kaucher arithmetic is an addition group and a conditionally complete lattice for multiplication.

With this in mind, the sequence of computational operations is set by the following algorithm.

Step 1. Set $t_0 = 0$ and $l = 0$. We set the initial approximations of the required parameters.

Step 2. Using the rules of Kaucher arithmetic, we find the external interval estimate for the derivatives

$$\frac{d\Delta U_C^P}{dt} = F_C^P(\Delta U_C^P) + V_1^C \Delta I_H^X + V_2^C \begin{bmatrix} \Delta U_R^P \\ \Delta I_R^X \end{bmatrix} + V_3^C J_C^P \cdot$$

Step 3. Find the interval expansion of the vector

$$\Delta U_C^P = \Delta U_C^P + \frac{d\Delta U_C^P}{dt} \times \Delta,$$ where Δ is the integration step.

Step 4. Solve the nonlinear interval system using the configuration method, which is a zero order method and does not require the calculation of interval derivatives

$$Z_X\left(\Delta I_H^X\right) = -B_C^H \Delta U_C^P + \left[-B_R^H \quad 0\right] \begin{bmatrix} \Delta U_R^P \\ \Delta I_R^X \end{bmatrix} E_H^X \cdot$$

Step 5. Solve the linear interval system using the well-proven Gaussian interval method

$$\left[\begin{array}{c|c} B_R^R & R_X \\ \hline Y_P & A_R^R \end{array}\right] \begin{bmatrix} \Delta U_R^P \\ \Delta I_R^X \end{bmatrix} = \begin{bmatrix} -B_C^R \\ 0 \end{bmatrix} \Delta U_C^P + \begin{bmatrix} 0 \\ -A_H^R \end{bmatrix} \Delta I_H^X - \begin{bmatrix} E_R^X \\ J_R^P \end{bmatrix}.$$

Step 6. Accept $l = l + 1$, $t_l = t_l + \Delta$.

Step 7. Is the process complete? If yes, go to step 8; otherwise - to point 2.

Step 8. End.

The results of calculating the characteristics of the inverter are shown in Fig. 6.

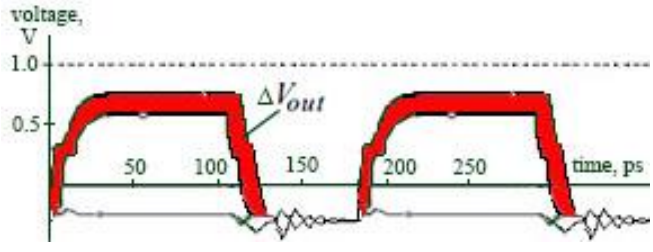

Fig. 6. The spread of the output voltage levels of the inverter in switching mode

V. Conclusion

The proposed method for studying the stability of nanoelectronic structures makes it possible to expand the range of use of devices based on quantum effects in various technical applications. A preliminary analysis of the robustness of tunnel-resonant heterostructures, a study of the features of their dynamic behavior and response to external influences, allows one to reduce the costs of computational and theoretical work when creating a structural layout of a product that ensures its operation under extended operating conditions. The developed set of interval mathematical models for the basic set of elements of tunnel-resonant heterostructures makes it possible to estimate the entire range of changes in the characteristics of the devices under study and to avoid enumerating all possible combinations of parameters when searching for the optimal option. The computational algorithms obtained in this work for calculating processes in a two-level logical cell MOBILE create prerequisites for expanding the field of application of resonant tunneling devices in high-speed monolithic integrated circuits.

References

[1] T.J. Slight, C.N. Ironside “Integration of a Resonant Tunneling Diode and an Optical Communications Laser”, IEEE, Photonics technology letters, 2006, vol. 18, № 14, pp. 1518-1520.

[2] J. Lee, S. Choi, J. Lee, K. Yang “40 Gb/s low-power 4:1 multiplexer based on resonant tunneling diodes”, IEEE Trans. Nanotechnol., vol. 11, № 5, pp. 890-895.

[3] X. Hu, G. Feng, S.Duan, L. Liu “Multilayer RTD-memristor-based cellular neural networks for color image processing”, Neurocomputing, 2015, vol. 162, pp. 150-162.

[4] P. Hillger, M. Van Delden, U. Thanthrige, et al. “Toward Mobile Integrated Electronic Systems at THz Frequencies”, J. of Infrared Millimeter and Terahertz Waves, 2020, vol. 41, № 7, p.846–869.

[5] J. Lee, S. Choi, S.-Y. Kim, J. Lee, K. Yang “Area-Efficient Series-connected Resonant Tunneling Diode Pair as Binary Neuron in Cellular Neural Network”, IEEE Electron Device Letters, 2020, vol. 41, Issue: 9, pp. 1308 - 1311.

[6] K. Lee, J. Yongsik “Temperature-dependent characteristics of a RTD-based microwave push-push oscillator”, Microwave and Optical Technology Letters, 2018, vol. 60, pp. 803-805.

[7] J.M. Quintana, M.J. Avedillo, J. Nunez et al. “Operation limits for RTD-based MOBILE circuits”, IEEE Transactions on Circuits and Systems, 2009, vol. 56(2), pp. 350-363.

[8] N. Maciej “Synthesis of multithreshold threshold gates based on negative differential resistance devices”, IET Circuits, Devices & Systems, 2013, vol. 7, Issue 5, p. 232 – 242.

[9] K. Maezawa, H. Sugiyama, S. Kishimoto, T. Mizutani “100 ghz operation of a resonant tunneling logic gate MOBILE having a symmetric configuration”, Proc. Int. Conf. Indium Phosphide and Related Materials, 2006, pp. 46–49.

[10] H. Shin-Ya, M. Suhara, N. Asaoka, M. Naoi “Implementation of Physics-Based Model for Current-Voltage Characteristics in Resonant Tunneling Diodes by Using the Voigt Function”, IEICE Transactions on Electronics, 2010, vol. E93.C, Issue 8, pp. 1295-1301.

[11] A.V. Bondarev, V.N. Efanov “Principles of the formation of a mathematical model of nano-electronic components of quantum computing systems with memresistive branches”, *Sistemy upravleniya i informatsionnyye tekhnologii*, (in Russian), 2020, №1 (79), pp. 4-10.

[12] G. Alefeld, G. Mayer “Interval analysis: theory and applications”, Journal of Computational Applied Mathematics, 2000, vol. 121, pp. 421-464.

[13] E. Kaucher “Interval analysis in the extended interval space IR ”, In: Alefeld G., Grigorieff R.D. (eds) Fundamentals of Numerical Computation (Computer-Oriented Numerical Analysis). Wien: Springer, 1980. – P. 33–49.